Supporting Information

Title: Supporting Information: Scalable, 'Dip-and-dry' Fabrication of a Wide-Angle Plasmonic Selective Absorber for High-efficiency Solar-thermal Energy Conversion

Jyotirmoy Mandal, Derek Wang, Adam Overvig, Nan Shi, Daniel Paley, Amirali Zangiabadi, Qian Cheng, Katayun Barmak, Nanfang Yu, Yuan Yang**

[*] Prof. Y. Yang and Prof. N. Yu, Corresponding-Authors.
Department of Applied Physics and Applied Mathematics, Columbia University,
Mudd 200, MC 4701, 500 W 120 Street, New York, NY 10027, U.S.A.
Email: yy2664@columbia.edu, ny2214@columbia.edu

J. Mandal, A. Overvig, N. Shi, Dr. A. Zangiabadi, Dr. Q. Cheng, Prof. K. Barmak, Prof. N. Yu*, Prof. Y. Yang*
Department of Applied Physics and Applied Mathematics, Columbia University,
Mudd 200, MC 4701, 500 W 120 Street, New York, NY 10027, U.S.A.

Dr. D. Paley
Department of Chemistry, Columbia University,
3000 Broadway New York, NY 10027

D. Wang
Department of Materials Science and Engineering, Durand Building, Stanford University
496 Lomita Mall, Stanford, CA 94305-4034, U.S.A.

1. Simulation Results

Simulated spectra used to obtain $\overline{\alpha}$, $\overline{\epsilon}$ and $\eta_{sol\text{-}th}$ in Figures 3c-e of the main text

Figure S1 depicts the simulation spectral absorptances $\alpha(\lambda)$ (= $\varepsilon(\lambda)$ = 1 – R(λ)) at normal incidence for various Cu nanostructure diameters *d* and layer thicknesses *h*, and for which $\overline{\alpha}$, $\overline{\epsilon}$ and $\eta_{sol\text{-}th}$ are presented in Figure 2c-e of the main text. For each *d*, the ribbons represent the spectral absorbance for some number of nanostructure layers of particles with a total height *h*. E.g. for *d* ~ 90 nm, 1 to 5 layers of Cu nanostructures on Zn are simulated, with 5 layers corresponding to *h* = 312 nm ~ 300 nm. As evident, for similar thicknesses *h*, layers with smaller *d* show a broader absorptance $\alpha(\lambda)$, leading to a higher $\overline{\epsilon}$. For larger particles with *d* ~ 90 nm or above, fluctuations in absorptance are seen in the 1-4 μm range, and are likely due to size-dependent resonances.

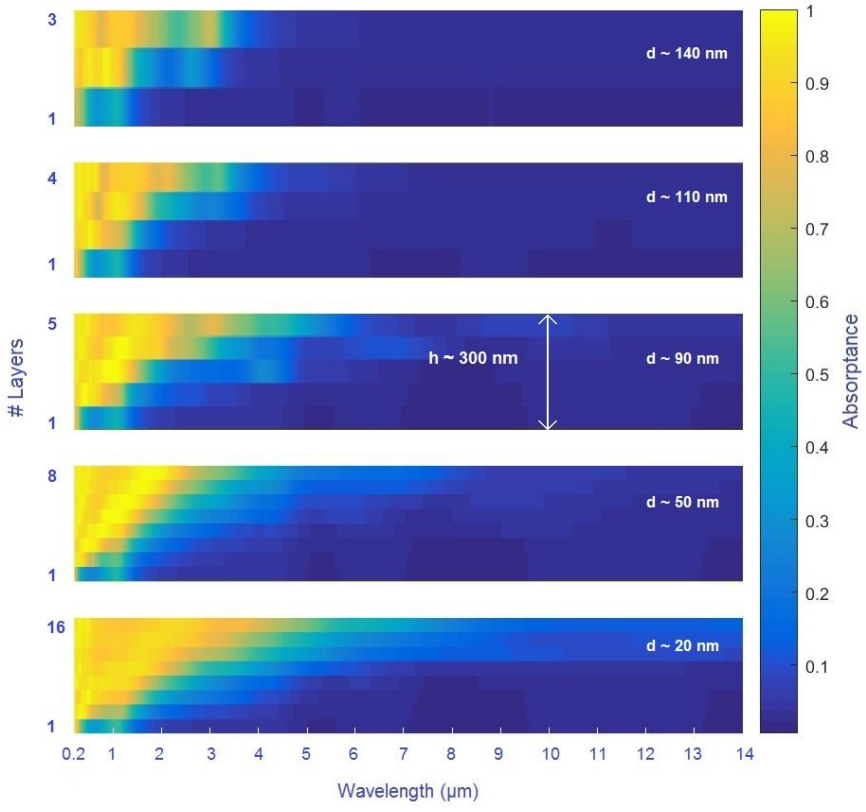

Figure S1. Color plots of the simulated spectral absorptances $\alpha(\lambda)$ (= $\varepsilon(\lambda)$ = 1 – R(λ)) at normal incidence for various Cu nanostructure diameters *d* and layer thicknesses *h*. For each value of *d*, a number of layers of nanostructures are simulated, with the highest number corresponding to *h* ~ 300 nm. The $\overline{\alpha}$, $\overline{\epsilon}$ and η_{sol-th} in Figure 2c-d of the main text is derived from $\alpha(\lambda)$ presented here.

Lossy effective medium behavior of the nanoparticle layer at thermal wavelengths

Figure S2 shows simulated absorptances at 4-14 μm wavelengths of freestanding layers of d = 20 and 90 nm nanostructures as a function of layer thicknesses h. Since the wavelengths are much larger than d, the nanostructure layer is expected to behave like an effective medium, and indeed, the rise in broadband absorptance with h indicates that the layer behaves like a lossy medium with poor reflectance in the thermal radiation wavelengths.

It should be noted that the nanostructures of the PNF have a variable range of sizes. Therefore, the spectral absorptance is likely to be a combination of the absorptances for different d values. In light of the simulation results presented here and in the main text, it is evident that those strongly corroborate the experiments.

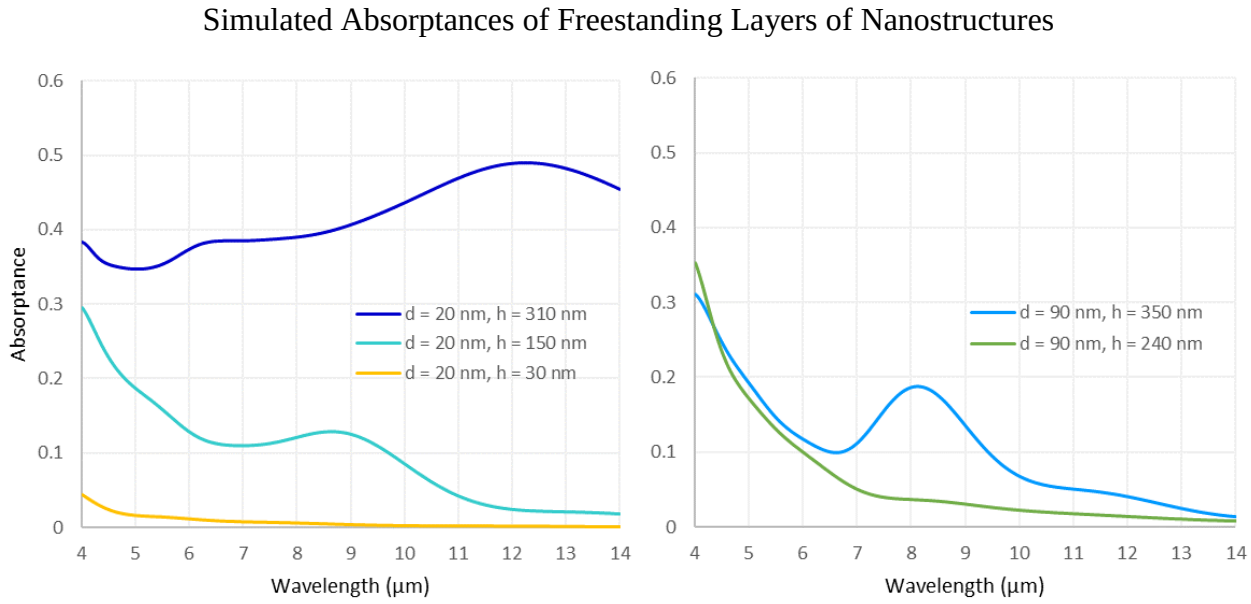

Figure S2. Simulated absorptances of free standing layers of Cu nanostructures (no zinc substrate present) for d = 20 and 90 nm. While the increase in absorptance is not exponential with thickness and peaks (such as the ones at 8 μm) potentially corresponding to resonances are observed, it is clear that a higher thickness corresponds to a greater attenuation of light. Essentially, the layer behaves as a lossy effective medium with a low reflectance.

Effect of Broadening the Nanoparticle Size-distribution

Figure S3 shows simulations of the effect of nanoparticle size distribution on the optical performance of the PNF. As shown in Section S5, for large size distributions, the large nanoparticles appear to 'sit' amidst a layer of smaller nanoparticles. Therefore, a layer of small nanoparticles (d ~ 50 nm, h ~ 100 nm) were simulated as a starting point. Then a layer of large d ~ 140 nm nanoparticles (~26 particles per μm^2) were dispersed over the first layer, and had its optical reflectance simulated. The simulation was then repeated with a layer of d ~ 200 nm particles (~10 particles per μm^2). In both cases, the added layer of larger particles had the same total nanoparticle volume. As evident, when the size-distribution is broader (~50-200 nm compared to ~50-140 nm), the absorption is broadened as well. While the already high $\overline{\alpha}$ shows a small relative change with nanoparticle size-distribution (0.82-0.83), $\overline{\epsilon}$ shows a significantly larger relative increase (0.036 to 0.056). As a result, η_{sol-th} drops from 0.78 to 0.77. The trend is similar to the experimental observations (Figure 4 of the paper), and lends support to the proposition that a broad nanoparticle size-distribution leads to a broadened absorption into the infrared, and consequently, a higher $\overline{\epsilon}$.

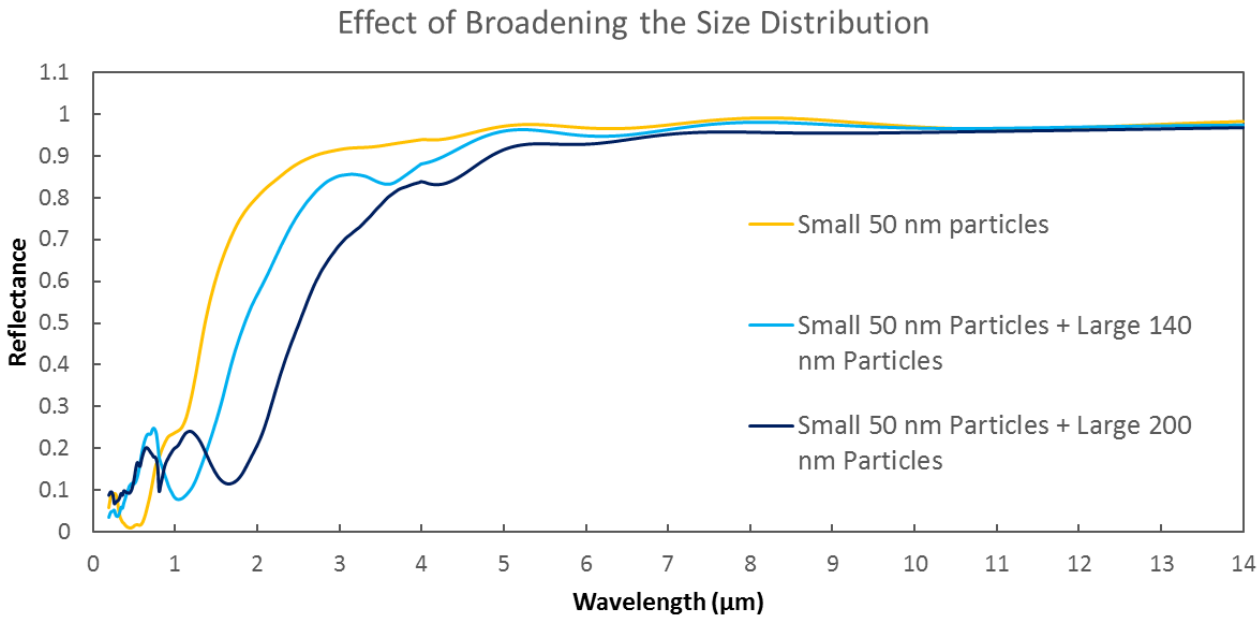

Figure S3: Simulations showing the effect of broadening the nanoparticle size-distribution on the spectral reflectance of the PNF.

2. Calculation of $\bar{\alpha}$ and $\bar{\epsilon}$ from Spectral and Simulated Reflectances

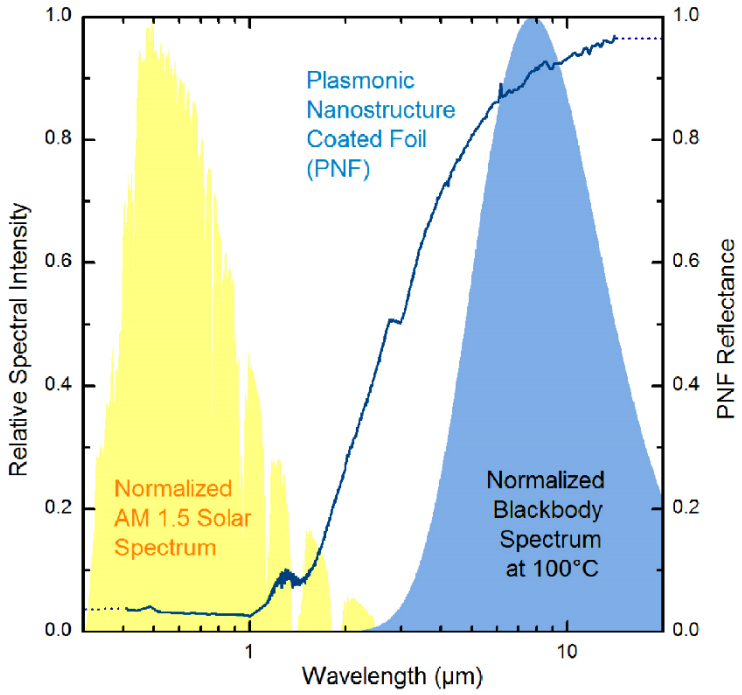

Figure S4. Extrapolations (dotted) of the spectral reflectance of the PNF to the ultraviolet and far-infrared wavelengths.

To calculate the solar absorptance and thermal emittance of the plasmonic nanostructure-coated foil (PNF), the measured and simulated spectral reflectances are extrapolated into the ultraviolet and far-infrared wavelengths as indicated in Figure S3. The reflectances of the left and right dotted lines correspond to average values of the reflectance over the 0.41-0.425 nm and 13-14 μm ranges respectively. Using the extrapolated spectrum and Equations 1, 2 and 3 in the main text, $\bar{\alpha}$ and $\bar{\epsilon}$ are calculated. From Figure S3, it appears that the extrapolation likely results in an overestimation of $\bar{\epsilon}$. On the other hand, $\bar{\alpha}$ is likely to be accurate, as the ultraviolet extrapolation is consistent with the simulated absorptances in the 0.3-0.41 μm range of the simulations in Figure S1.

3. Normal Incidence Correction of the ASTM 1.5 Global Spectrum

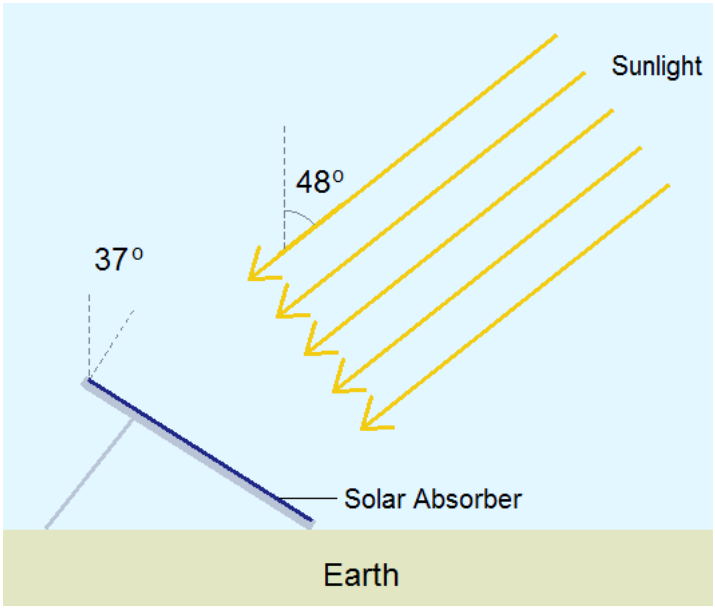

Figure S5. Schematic of the setup for which the AM 1.5 Global Solar Intensity spectrum is defined.

As shown in Figure S4, the AM 1.5 Global Solar Intensity Spectrum (ASTM G173-03) is defined for sunlight coming an angle of incidence (zenith angle) of 48° and a surface tilted at 37° from the normal. Therefore, the normal incidence correction, which corresponds to the surface adjusted to perpendicularly intercept the sunlight, requires a 11° angular correction of the direct component of the sunlight (900.1 Wm^{-2} out of a total intensity of 1000.4 Wm^{-2}). The diffuse component comprising of scattered light from the sky and earth is a function of the environment, and is assumed to be constant. It is also assumed that the scattered and diffuse components have identical normalized spectra, i.e. they differ only by total intensity. With these considerations, the normal incidence-corrected intensity is calculated as:

$$I_{solar,0°} = \frac{I_{direct}}{\cos((48-37)°)} + I_{diffuse} = \frac{900.1}{\cos(11°)} + 100.3 = 1017\ Wm^{-2} \quad \text{(S.1)}$$

The intensity corrections for other angles can be similarly calculated.

4. Variation of the Angle of Incidence of the Sun with Time of the Day and Year

Figures S5 show the variation in the solar incidence (zenith) angle over New York (40.7128° N, 74.0059° W) and New Delhi (28.6139° N, 77.2090° E), two urban centers representing different demographics, economies and climate, and whose latitudes span areas with large populations which can benefit from solar-heating.[1] As evident, even in the summer, for both locations, the sun remains high in the sky (angle of incidence < 50°) for only half of the daylight hours. During the equinoxes, thay duration decreases further, and during the winter, the sun does not rise appreciably high in the sky at all. Furthermore, the seasonal variation in the zenith angles are also significant, with the angle of the sun varying by ~48° in both cities over the period of a year. While a flat plate solar collector can have its angle optimized to harvest solar energy depending on its location, it is evident that for fixed configurations, a wide angle solar absorptance is necessary to efficiently harvest sunlight over daylight hours and across seasons.

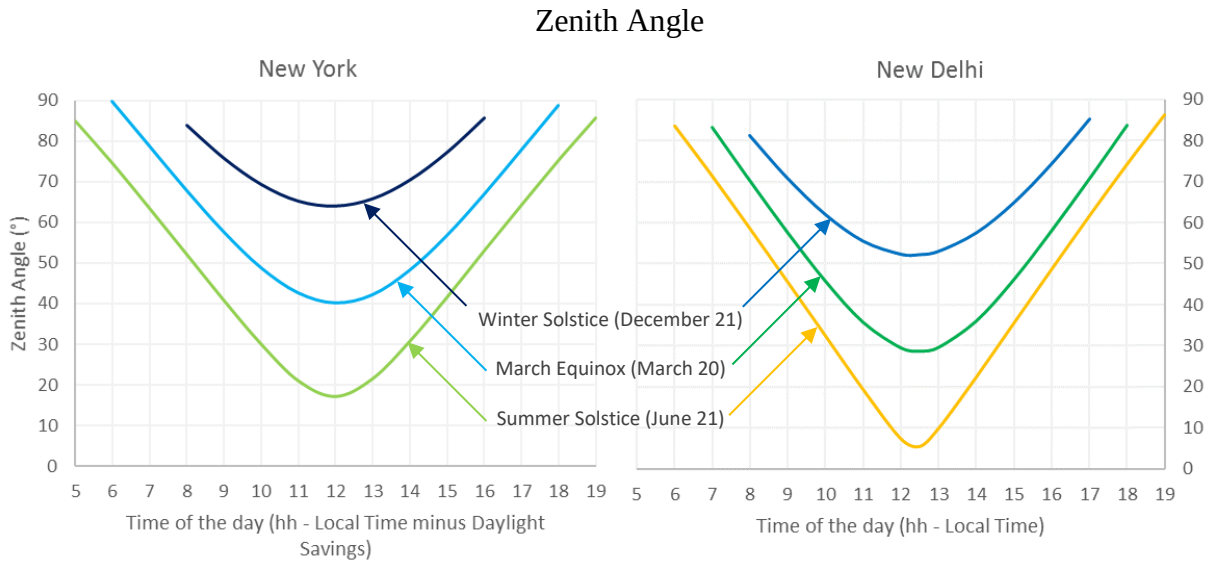

Figure S6. The variation of the incidence angle of the sun with time of day and year in New York and New Delhi.

5. Variations of Nanostructure Diameters *d* with Cu^{2+} Concentration, Reaction Time and Temperature: SEM Images and Statistics

Table 1. SEM images and diameter (*d*) distributions of the plasmonic Cu nanostructures deposited on Zn under various reaction parameters. The 'standard set' of parameters is taken as [Cu^{2+}] = 12.5 mM, Time = 30s and Temperature = 22°C, and reaction parameters are varied one at a time (marked in light blue) from that set. Scale bars in the SEM images represent a length of 200 nm. Means μ_d and standard deviations σ_d of the distributions are presented in Figures 3g-i of the main text.

SEM Image	**Distribution of nanostructure diameter *d* (nm)**
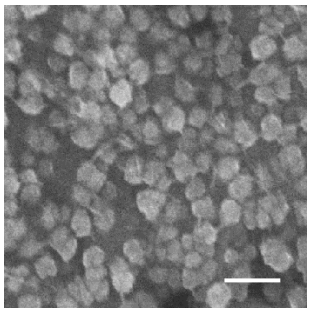 **$CuSO_4$ (aq) 12.5 mM, 15s, 22°C**	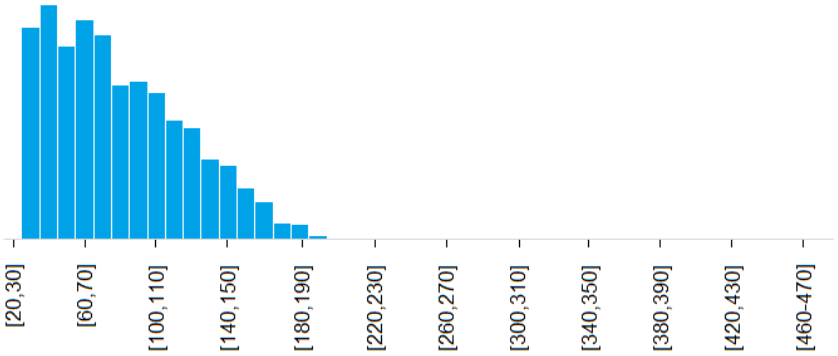
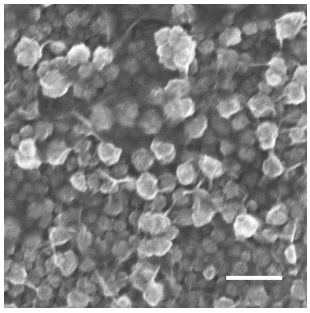 **$CuSO_4$ (aq) 12.5 mM, 30s, 22°C**	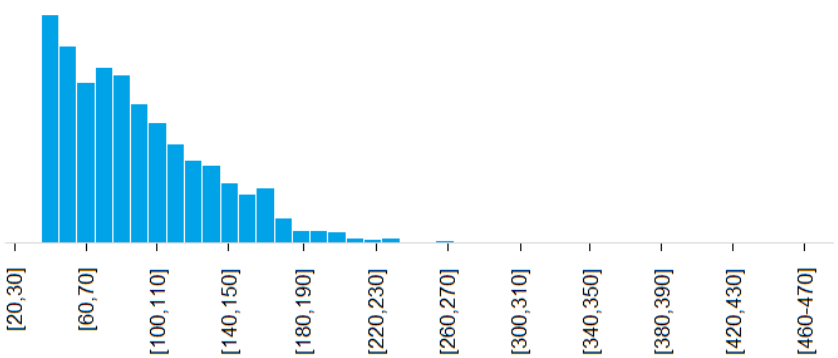
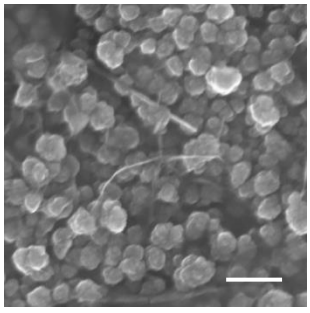 **$CuSO_4$ (aq) 12.5 mM, 45s, 22°C**	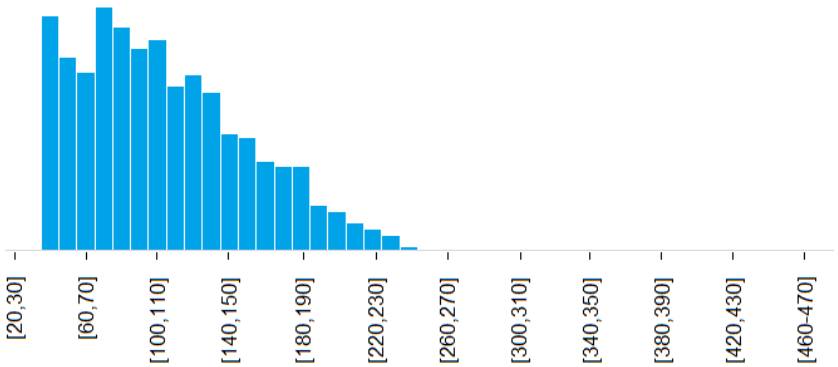

SEM Image **Distribution of nanostructure diameter *d* (nm)**

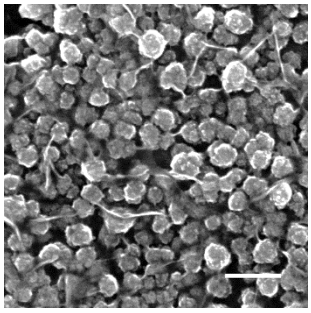

$CuSO_4$ (aq) 12.5 mM, 30s, 0°C

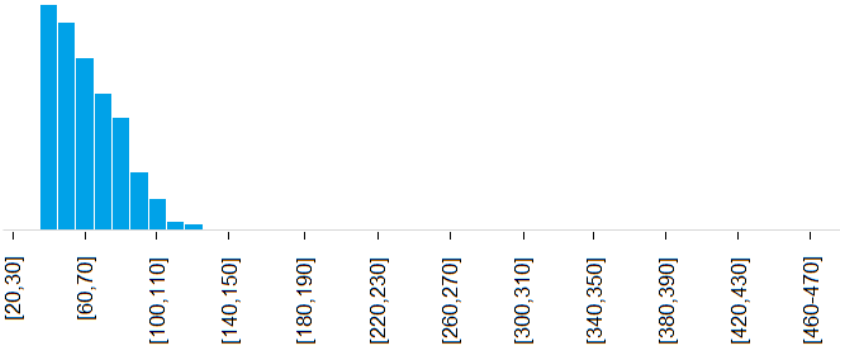

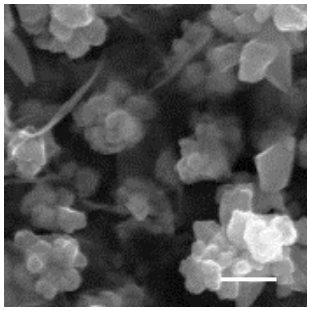

$CuSO_4$ (aq) 12.5 mM, 30s, 75°C

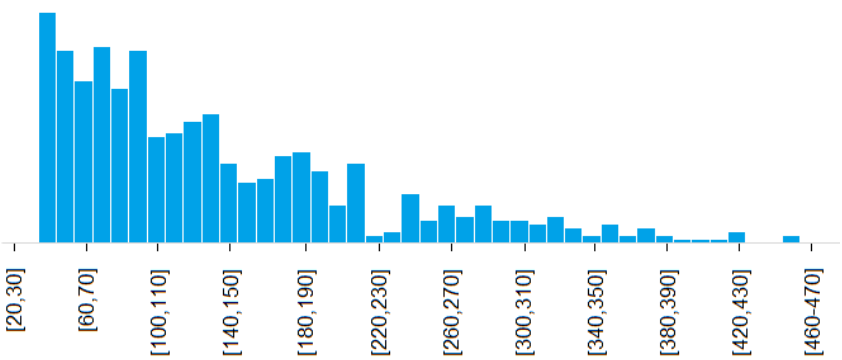

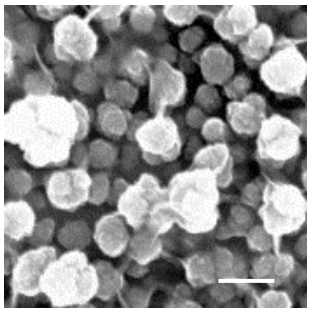

$CuSO_4$ (aq) 25 mM, 30s, 22°C

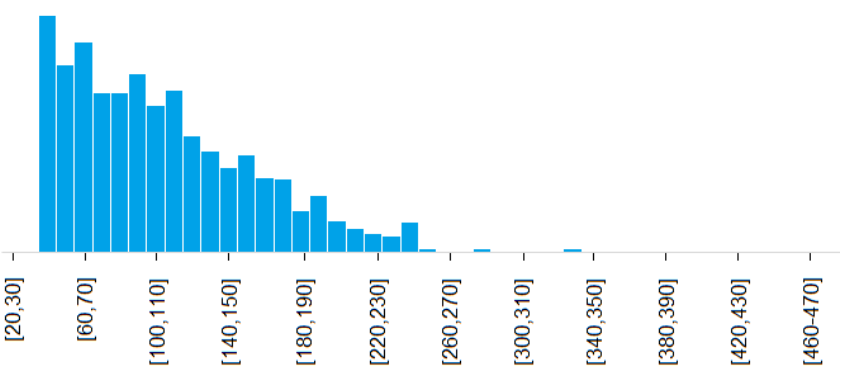

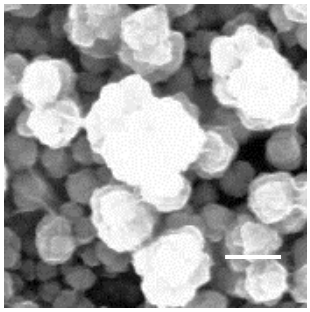

$CuSO_4$ (aq) 50 mM, 30s, 22°C

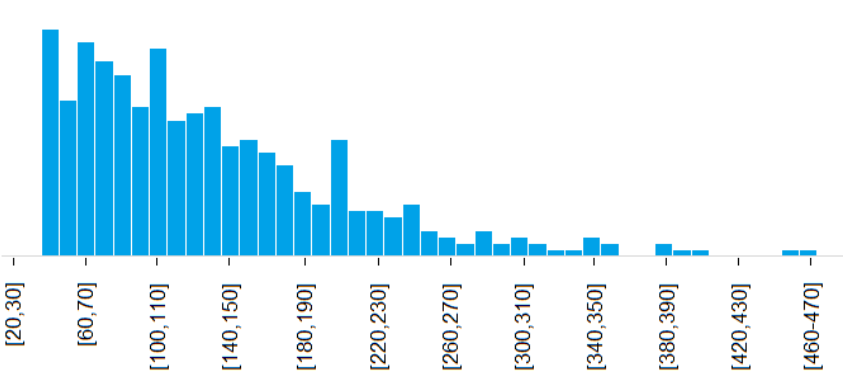

6. Variation of Nanostructure Layer Texture with the Type of Deposition of Metal

To investigate the effect of the type of metal deposition on nanostructure surface features of the deposited nanostructures, continuous depositions of copper on zinc and silver on zinc, as well as sequential and co-depositions of copper and silver on zinc were carried out. Figures S6 and S7 show the different nanostructures obtained and selected reflectance spectra. It is also observed that for prolonged depositions of silver, the nanostructures grow into dendrites – a well-known phenomenon.[2] Reflectance spectra of PNFs fabricated from the depositions indicate that the variants show similar optical properties as the copper-zinc pair described in the main text.

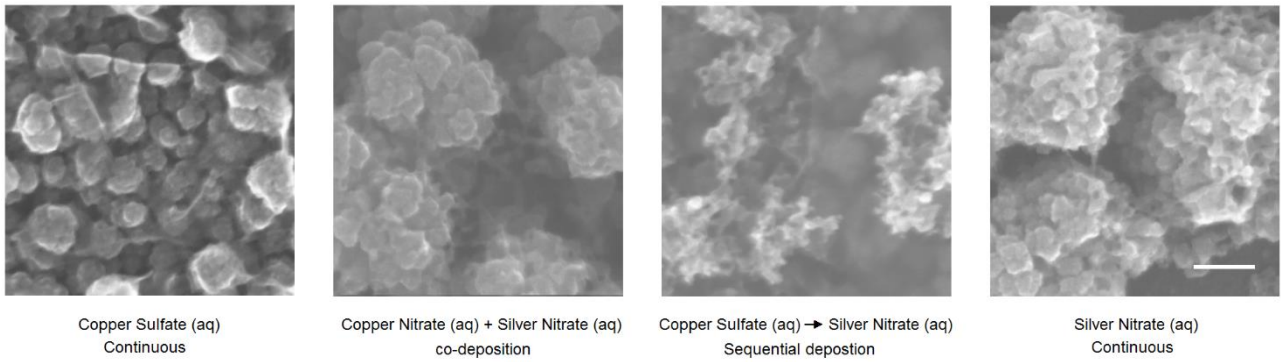

Figure S7. Different textures formed by continuous single deposition, co-deposition and sequential depositions of copper and silver nanostructures on zinc. Scale bar represents a length of 100 nm.

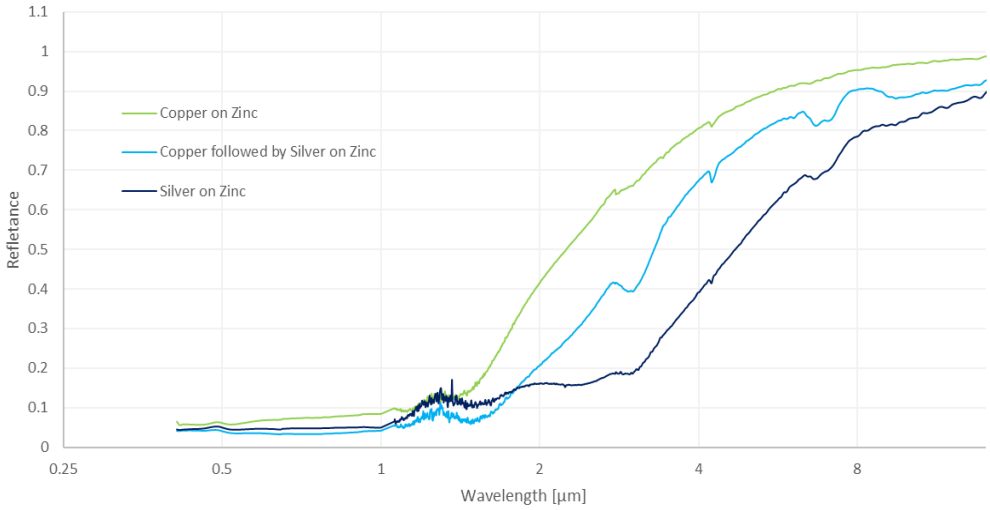

Figure S8. Spectral reflectances of individual and sequential depositions of copper and silver on zinc.

7. Solar Simulator Test

Figure S8 shows the setup for the solar simulator test. During the experiment, the lamp was found to heat up the air considerably, so a fan was used to maintain a draft (not blowing near the sample) to cool the lamp and keep the air at the midpoint between the sample and the lamp at 29°C. The temperatures of the surrounding walls within a 4 feet height of the PNF were measured at ~30°C, while that of the lamp's glass was found to be ~170°C. From those values and a rough estimation of the view factors for the PNF, an effective 'sky temperature' > 30°C was calculated. Earlier, a thermopile sensor (type 3A, item 7Z02621, Ophir Photonics) was used to adjust the intensity of the lamp such that the 'solar' irradiance at the location of the PNF, and after transmission through poly(ethene), was equal to that of the AM 1.5 Global Solar Spectrum ($\pm$1%). The thermal irradiance from the lamp after transmission through poly(ethene) was also measured, and was found to be small (~1.5%) relative to the solar component, and therefore not considered to be significant.

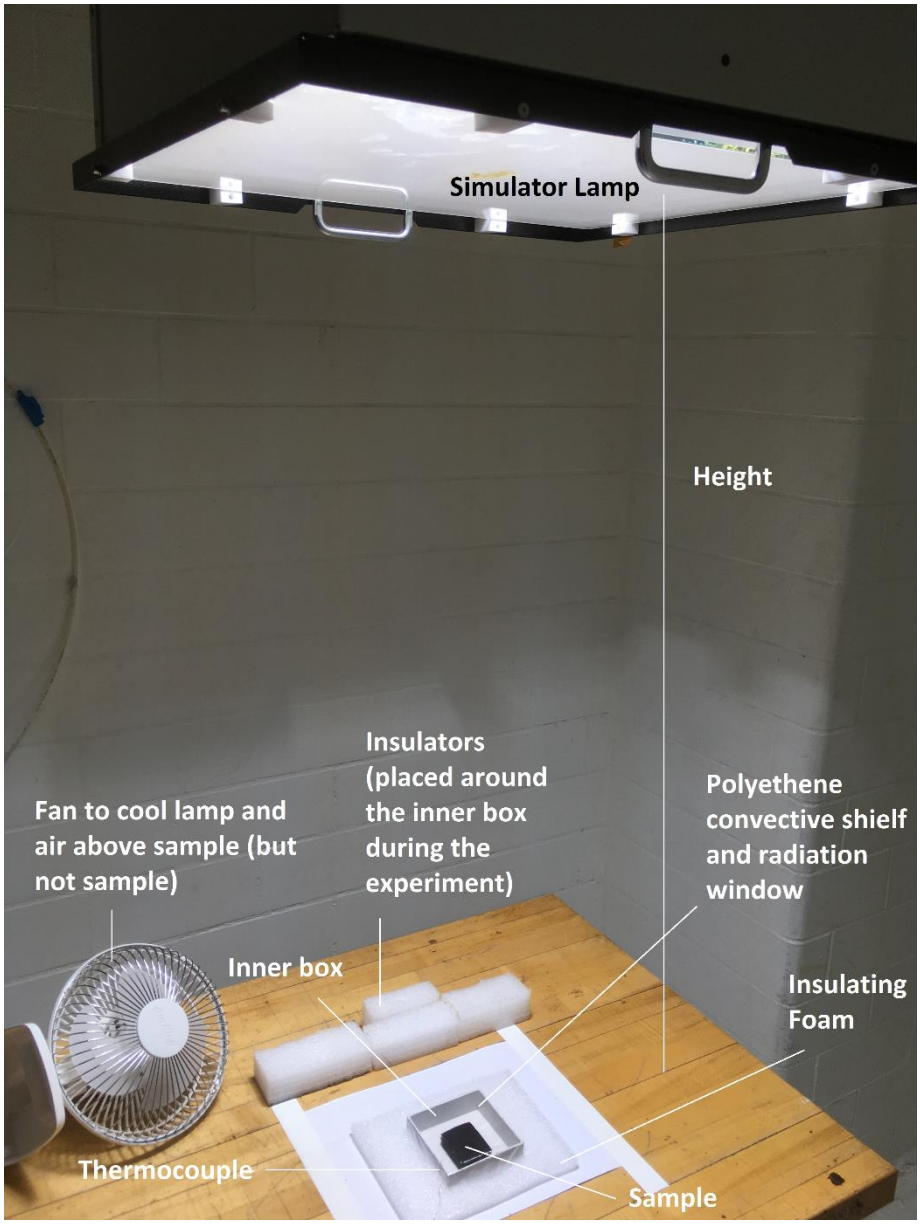

Figure S9. The solar simulator setup. It should be noted that the fan was brought into view of the camera for the picture. During the experiments, the fan was placed further, and directed at the lamp.

8. Stability Test Results

Mechanical Stability of the PNF

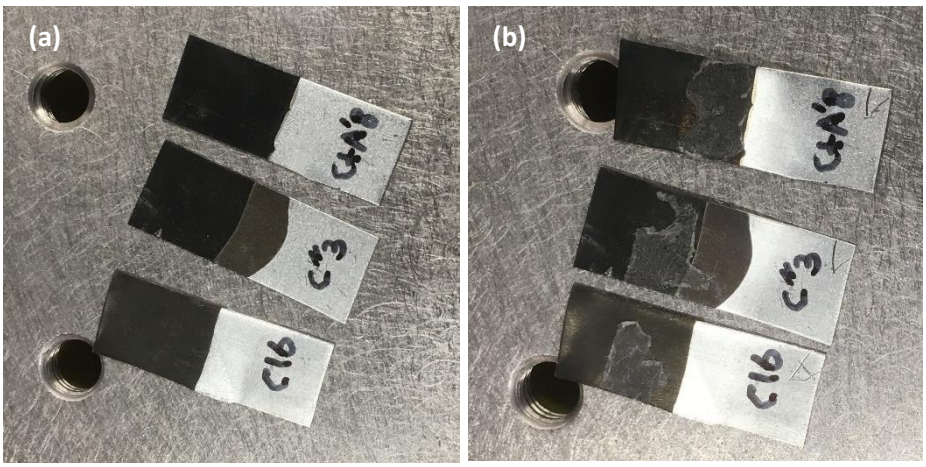

Figure S10. Pictures of variants of the PNF (a) before and (b) after ASTM D3359-09 adhesion tests. As observed, the tape remains on the samples during the peel-off, indicating a high mechanical stability of the samples.

Thermal Stability of Copper Particles and the PNF

Figure S11a shows X-Ray diffraction (XRD) peaks of pristine and heat treated (24 hours in air at 100°C) Cu particles extracted from the PNF (as described under "Material Characterizations" in the Experimental Section, to get rid of the overwhelming signatures of the Zn substrate). As shown, even after prolonged heating at 100°C, the only discernable peaks are those of copper. The particles are likely to be even more stable when on the PNF, as the Zn substrate, being more reducing than Cu, could "galvanize" the Cu NPs from oxidation. Indeed, Auger electron spectra taken at different depths of the pristine and heat-treated PNFs (24 hours in air at 100°C) show a clear copper trace within a depth $\lesssim$ 20 nm (Figure S11b). Evidently, the oxidation is limited within $\lesssim$ 20 nm from the PNF's surface, a small value compared to the thickness (~200-400 nm) of the nanostructure layer. Along with the XRD data, this strongly indicates that the PNF is thermally stable even under operation in air.

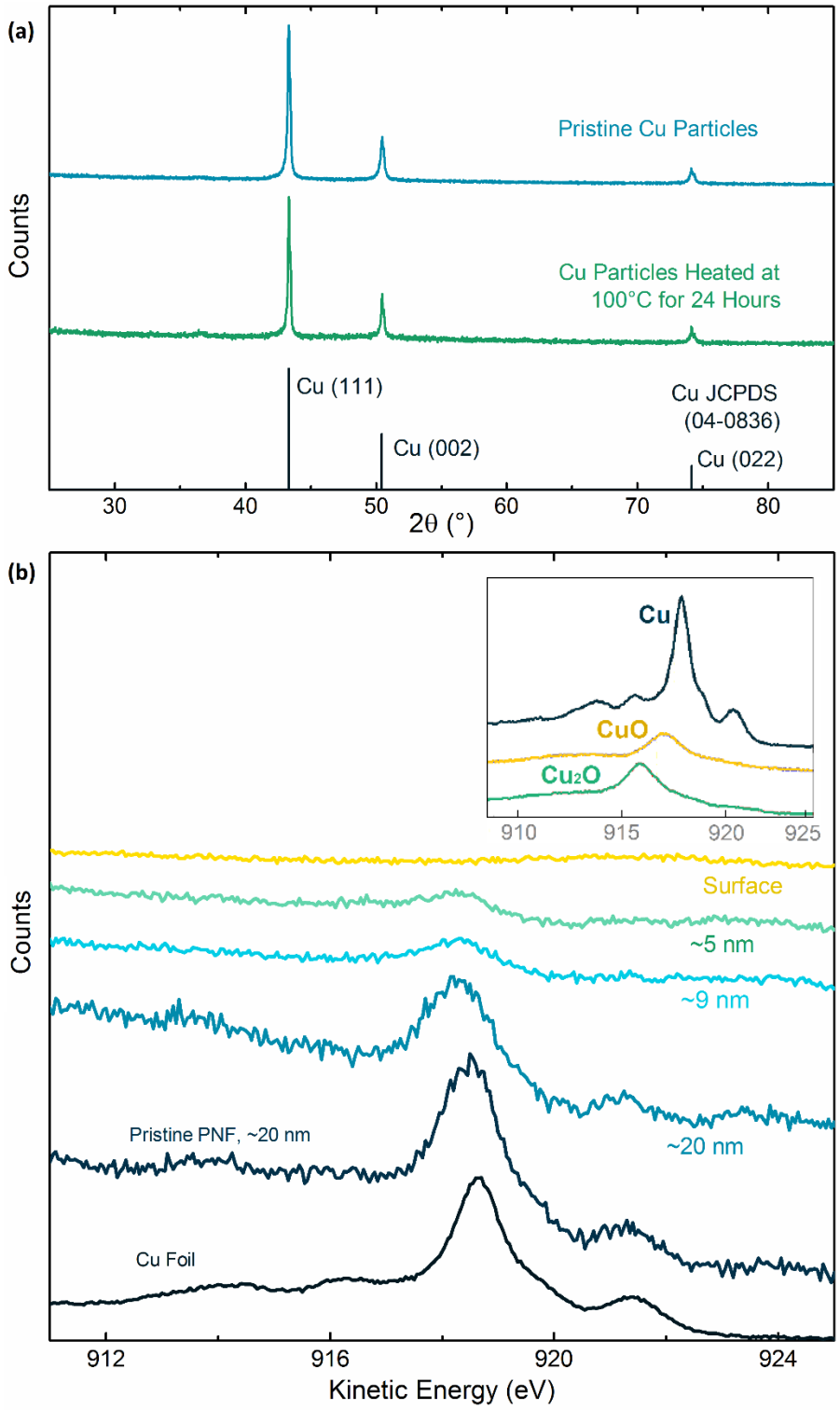

Figure S11. a) X-Ray diffraction plots of pristine and heat treated (24 hours in air at 100°C) Cu particles. b) Auger spectra of a pristine and a heat-treated (24 hours in air at 100°C) PNFs at different depths, and of a reference Cu foil that had surface oxide removed. The inset shows Auger spectra of Cu and Cu_xO reported in literature.[3]

Scanning Electron Micrographs of Samples Undergoing Thermal Stability Tests

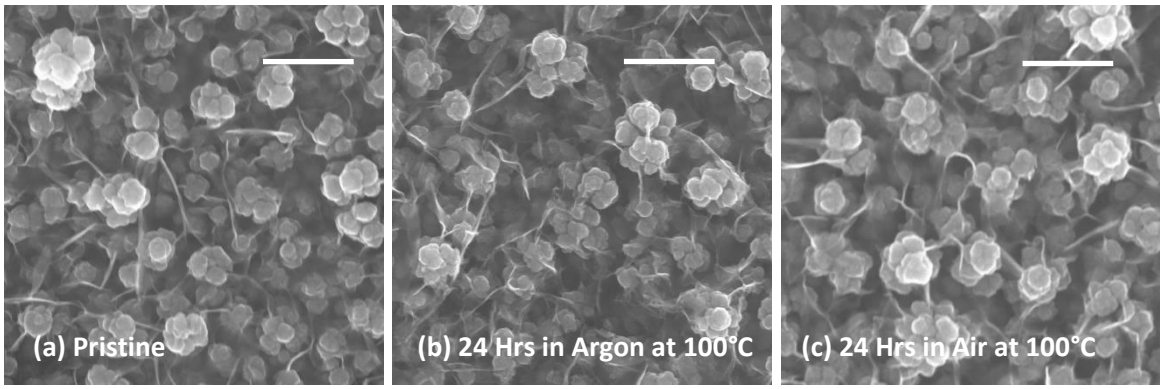

Figure S12. Scanning electron micrographs of PNFs made using same reaction parameters (a) in pristine state, (b) after heating for 24 hours in Argon at 100°C, and (c) after heating for 24 hours in Air at 100°C. Scale bars represent a length of 400 nm. As evident, the morphology is stable under thermal stresses.

9. Possibility of Using Other Substrates

While the copper nanostructures described in the paper were deposited on pure Zinc foils, it is in fact possible to use other substrates as well, as long as they are coated by zinc. Figure S10 shows a piece of aluminum foil, which was first coated with Zinc using a double zincate immersion method, and then dipped in aqueous copper sulfate. The resulting PNF is found to be suitable for selective solar absorption. A similar phenomenon is observed for galvanized steel.

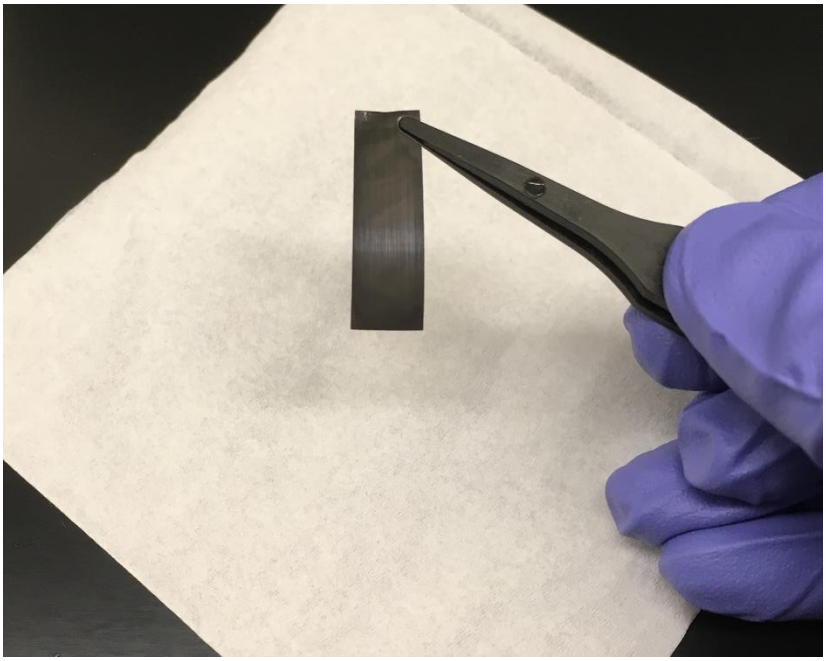

Figure S13. Photograph of a copper nanostructure-coated Aluminum foil, which was coated with a layer of zinc before nanostructure deposition.

References

[1] M. Kummu, O. Varis, *Applied Geography* **2011**, *31*, 495.
[2] A. Gutés, C. Carraro, R. Maboudian, *J. Am. Chem. Soc.* **2010**, *132*, 1476.
[3] T. Dahlang, T. Sven, *J. Phys.: Condens. Matter* **2012**, *24*, 175002.